Contents

S1 Viscosity measurement

We used the micropipette aspiration technique to measure the viscosity of the PSM following the same approach as in [1]. Explants of the presomitic mesoderm (PSM) were prepared with the procedure described in [2]. At a constant aspiration pressure, ΔP, the explant advances in the capillary as is shown in Fig. S1(A). The viscosity, η, is related to the flow of the explant inside the capillary via the expression $\eta = F_a/3\pi\dot{L}$, where F_a is the aspiration force given by $F_a = R_p^2\Delta P$ (here we do not consider the effect of the surface tension), where R_p is the radius of the pipette, and $\dot{L}$ is the constant flow velocity corresponding to the slope of the aspiration curve in Fig.S1(B). This yields an estimate for the viscosity given by $\eta \sim 10^4$ Pa.s.

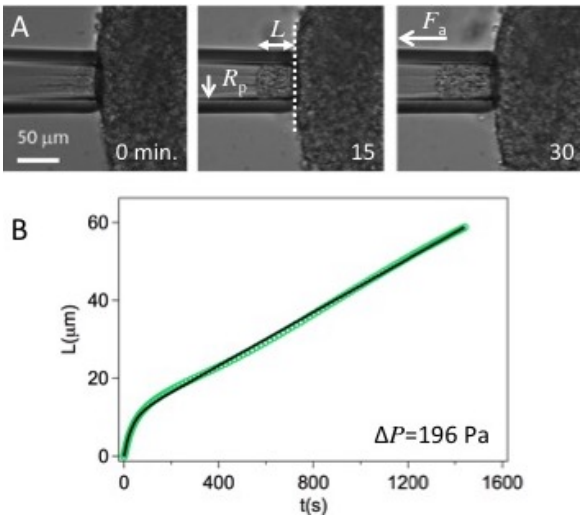

Fig. S1. Pipette aspiration to measure the viscosity of the PSM. (A) Timelapse of the aspiration of the middle section of a PSM explant (B) Aspiration curve corresponding to (A).

S1.1 PSM friction with the walls

To evaluate the friction coefficient between the PSM and the surrounding tissues (neural tube, lateral plate, ectoderm and endoderm), we use an ex-vivo approach where an explant of PSM is forced to move inside an uncoated glass capillary under the action of an external aspiration force (Fig. S2(A)). The non-specific adhesion between the explant and the glass capillary mimics the friction between the PSM and its surrounding in-vivo.

The friction coefficient of the tissue with the walls is measured by probing the advancement of the PSM explant inside the capillary at a constant aspiration pressure, ΔP. As before, the aspiration force is $F_a = \pi R_p^2 \Delta P$. The friction force is $F_f = 2\pi R_p L_{exp} k v$, where k is the friction coefficient and L_{exp} is the length of the explant. Balancing F_a with F_f gives: $\frac{R_p \Delta P}{L_{exp}} = 2kv$. We perform the experiment on explants of PSM with variable sizes and from the slope of the fitted line in Fig. S2(B), obtain $k = (1,8 \pm 0.4) \times 10^8$ N.s/m^3, where we note that k is depth-integrated parameter. Therefore, the bulk friction coefficient ξ scales as $\xi \approx k/w$, where $w \approx$100 μm is the width of the PSM, giving $\xi \sim 10^{12}$ N.s/m^4.

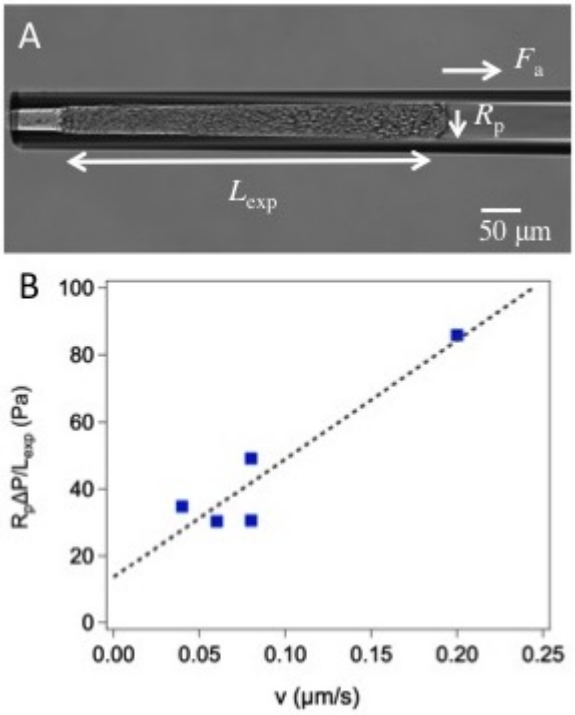

Fig. S2. Friction coefficient measurement. (A) Sliding of a PSM explant inside a capillary under a constant aspiration force. (B) The slope gives an average k from several experiments.

Table S1. The list of parameters for our microscopic-model to solve Eq. [2-8] of the main text.

$\mathcal{D}$	k	a	γ	τ	ρ_0
$0.1, 0.5, 2.5$	100	1	50	$50, 100, 200$	$0.16, 0.24, 0.32, 0.4$

Table S2. The list of extracted scales from the experimental data and the continuum model. We are reporting the estimate of diffusivity $\mathcal{D}$, decay lengthscale of motility L, decay length scale of the drif velocity L_v, length scale set by the ratio of viscous to friction dissipation l_ξ and velocity-scale V in the dimensional form.

$L(\mu m)$	$L_v(\mu m)$	$l_\xi(\mu m)$	$V(\mu m/s)$	$\mathcal{D}(\mu m^2/s)$
1280	1400	1800	0.026	0.08

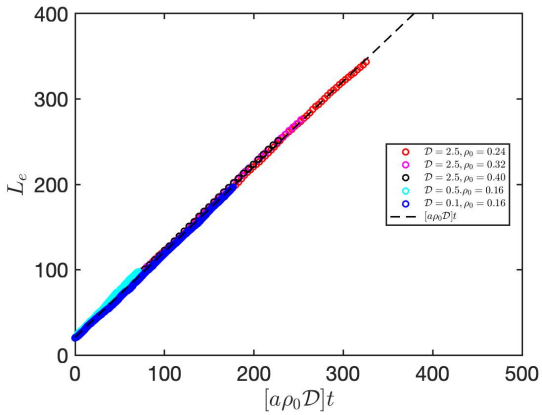

Fig. S3. Microscopic cell-based simulation: Elongation of PSM as a function of rescaled time for different value of $\mathcal{D}$ and ρ_0. These results are obtained by solving Eq. [2-8] of the main text.

S2 Microscopic cell-based simulations

We carried out several simulations with various values of the cell diffusivity $\mathcal{D} = 0.1, 0.5, \& \ 2.5$ and maximal cell packing $\rho_0 = 0.16, 0.24, 0.32, \& \ 0.4$. In Fig. (S3) we plot the position of TB (L_e) vs rescaled time ($a\rho_0\mathcal{D}t$), where t is simulation time and a is the cell size. All the curves from the microscopic model simulation with different $\mathcal{D}$ and ρ_0 values collapse to the dashed line with slope 1. This indicates that the elongation rate $V = a\rho_0\mathcal{D}$, consistent with the simple scaling estimate in the main text (Eq. 9, Main Text).

In Fig. (S4) we show the drift velocity v(x) and diffusivity $D(x)$ profiles from the microscopic model for $\tau = 50$ that was shown in the main text Fig.2C-D, x-axis of the mmicroscpoic model is rescaled by the appropriate

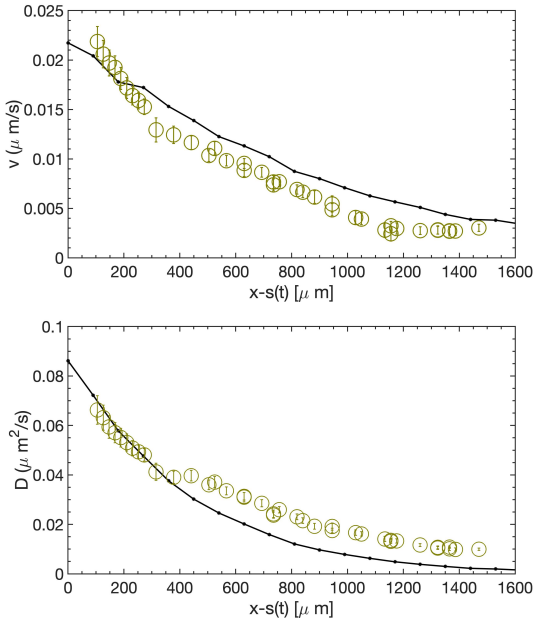

Fig. S4. Microscopic cell-based simulation: Experimentally mea-sured velocity v(x) and diffusivity $D(x)$ profiles (calculated using Eq. [1], open circles) as a function of distance from the TB compared to the rescaled numerical results of our-agent based model (black line with dots). These results are obtained by solving Eq. [2-8] of the main text.

length scale $25.6\mu m$, i.e., $x = 25.6x_{\text{Simulation}}$ (from microscopic model $L = 50$ and from the experimental data $L \sim 1280\mu m$), and y-axes are rescaled by maximal velocity ($\sim 0.026\mu m/s$) and maximal diffusivity ($\sim 0.08\mu m^2/s$), respectively, obtained from the experimental data and is compared it against the actual experimental points. $x_{\text{Simulation}}$ is in the microscopic simulation unit. Given that the simulation data comes from a minimal microscopic model with simplistic interaction potentials, the profiles agree reasonably well.

Table S1 summarizes all the parameter values used for our microscopic-model to solve Eq. [2-8] of the main text.

Run	Π_1	Π_2	Π_3	Π_4	Π_5
R1	0.01	2	1	0.003	0.005
R2	0.1	2	1	0.003	0.005
R3	0.01	2	10	0.003	0.005
R4	0.01	20	1	0.003	0.005
R5	0.01	0.2	1	0.003	0.005
R6	0.01	2	1	0.0	0.005
R7	0.01	2	1	0.003	0.001
R8	0.01	2	1	0.003	0.05
R9	0.01	100	100	0.003	0.05
R10	0.1	10^{-3}	100	0.003	0.05

Table S3. The list of dimensionnless parameters, scaled cell size $\Pi_1 = \frac{a}{L}$, scaled active stress $\Pi_2 = \frac{\alpha\rho_0}{\xi V^2\tau}$ (active stress/external friction), scaled internal viscosity $\Pi_3 = \frac{\eta}{\alpha\rho_0\tau}$, and the parameters corresponding to boundary condition $\Pi_4 = \frac{F}{\alpha\rho_0}$, $\Pi_5 = \frac{\mathcal{D}}{\mathcal{R}V\tau}$. These parameters are used for the sensitivity analysis of our macroscopic model.

S3 Macroscopic continuum model

In Table S2, we are reporting the estimate of diffusivity $\mathcal{D}$, decay lengthscale of motility L, decay length scale of the drif velocity L_v, length scale set by the ratio of viscous to friction dissipation l_ξ and velocity-scale V in the dimensional form.

Table S3 shows the range of dimensionless parameter values used in solving the eq (16)-(20), with the aim of the sensitivity of the results to these choices. R1 corresponds to the reference case used to fit the experimental data; the remaining set has one parameter which has been changed with respect to the set R1 for sensitivity analysis of our macroscopic model.

In Fig. S5, we show that an exponential profile (dashed red line) for both the velocity and the diffusivity fits well with the experimental data and the model in the posterior region close to the TB, with some expected deviation in the anterior region (run R1 of Table S3, Eq. [16-20]). The characteristic decay length for the diffusivity is $L = 1280\mu m$, while that for the velocity is $L_v = 1400\mu m$.

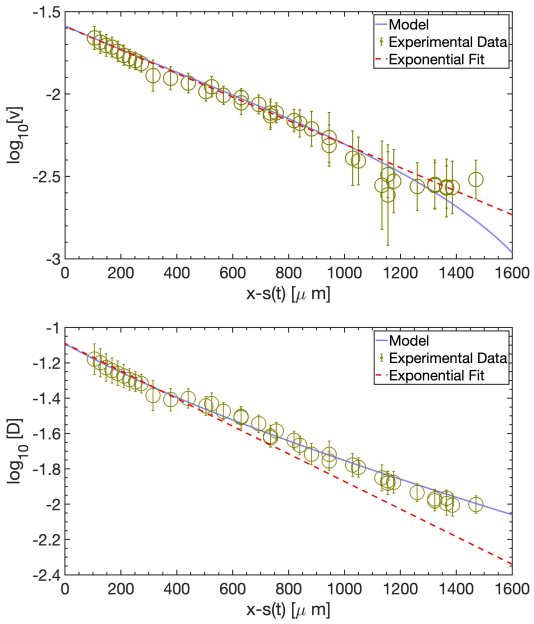

Fig. S5. Macroscopic continuum model: Log-lin fit for velocity and diffusivity profile along AP for run `R1` of Table S3. These results are obtained by solving Eq. [16-20] of the main text.

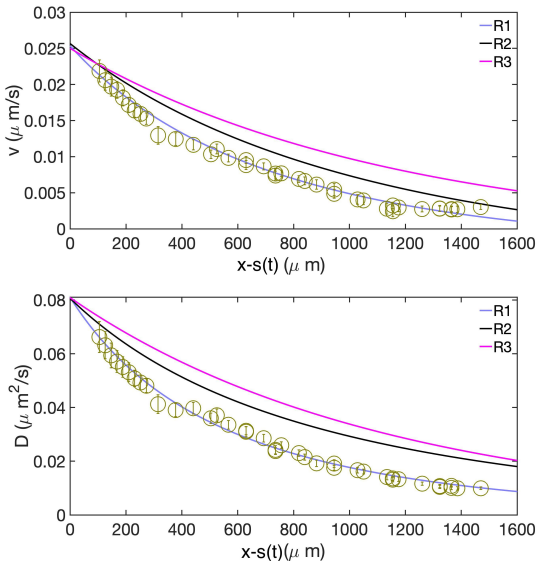

Fig. S6. Macroscopic continuum model: The velocity and diffusivity profile for varying scaled cell size (Π_1) and scaled internal viscosity (Π_3) run `R2, R3` of Table S3. These results are obtained by solving Eq. [16-20] of the main text.

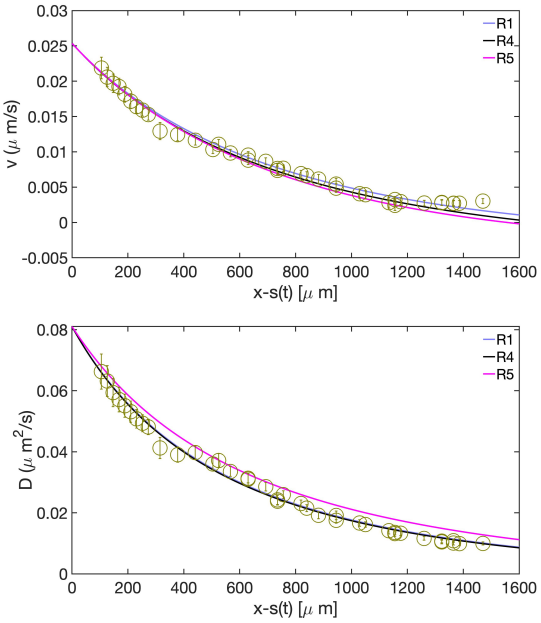

Fig. S7. Macroscopic continuum model: The velocity and diffusivity profile for varying scaled active stress (Π_2) run `R4, R5` of Table S3. These results are obtained by solving Eq. [16-20] of the main text.

S3.1 Dependence of solution on the dimensionless parameters

In Fig. S6, we see that the spatial profile of diffusivity and velocity becomes flatter with an increase in the scaled cell size Π_1 (run `R2` of Table S3). A similar trend is observed for the increase in the scaled internal viscosity Π_3 (internal viscosity/active stress) for run `R3` of Table S3.

In Fig. S7, we plot the spatial profile of velocity and diffusivity as a function of the scaled active stress $\Pi_2 = 20$ & 0.2 (active stress/external friction) (run `R4, R5` of Table S3 (Eq. [16-20])). Overall the change in the scaled external friction coefficient does not have a significant effect and the velocity and diffusivity profile is within the error-bars of the experimental data.

In Fig. S8, we show the effect of boundary conditions on the spatial profile of diffusivity and velocity associated with variations in Π_4, Π_5 run `R6, R7, R8` of Table S3 (Eq. [16-20]). Overall we see that the change in

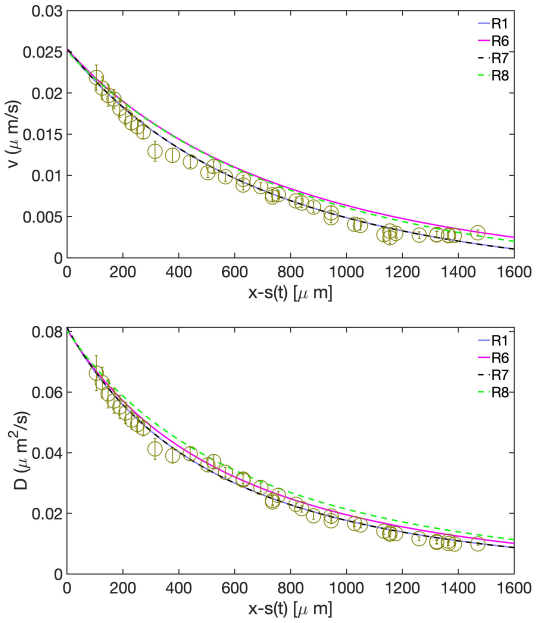

Fig. S8. Macroscopic continuum model: The velocity and diffusivity profile for varying boundary conditions (Π_4) and viscosity (Π_5) for run `R6`, `R7`, `R8` of Table S3. These results are obtained by solving Eq. [16-20] of the main text.

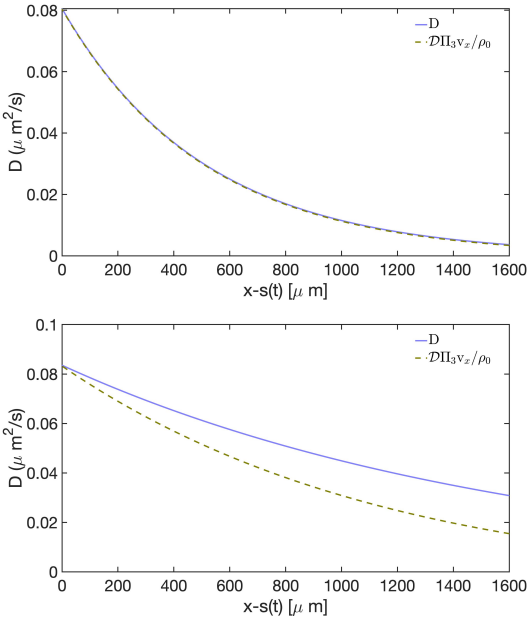

Fig. S9. Macroscopic continuum model: Plot of Diffusivity D and $\mathcal{D}\Pi_3 v_x/\rho_0$ vs distance from the TB to compare the density of motile cells $\rho(x)$ and velocity gradient $v_x(x)$ for run `R9` (top panel) and `R10` (bottom panel) of Table S3. These results are obtained by solving Eq. [16-20] of the main text.

boundary conditions does not affect the profile significantly and the velocity and diffusivity profile is within the error-bars of experimental data.

In Fig. S9, we plot the diffusivity $D(x) = \rho(x)\mathcal{D}/\rho_0$ and $\mathcal{D}\Pi_3 v_x/\rho_0$ profiles for two extreme values of scaled active stress $\Pi_2 = 100$ & 10^{-3} (active stress/external friction) (run `R9-R10`Table S3). These plots will give us a comparison between the two contrbution in LHS of Eq. [17], i.e., density of motile cells $\rho(x) = D(x)\rho_0/\mathcal{D}$ and $\Pi_3 v_x$. From Eq.(17) one can deduce that for very large values of Π_2 the friction term will be relatively small, and therefore the density $\rho(x)$ will track $\Pi_3 v_x$ as can be clearly seen (Run `R9`, top panel Fig. S9). For small values of Π_2, all the terms in Eq. (17) are comparable to each other and so there is no simple relation linking the density and the velocity gradient (Run `R10`, bottom panel Fig. S9).

S3.2 Phase Diagram

For the range of parameters where we find a good agreement of the macroscopic model with experimental results, i.e., run `R1` of Table S3, we have seen that the parameters Π_1 and Π_3 affect the velocity $v(x)$ and motility $\rho(x)$ profile significantly. In Fig. S10 we show a phase diagram of the length scale corresponding to the exponential fall in the density of motile cells L (top panle) and the length scale corresponding to the exponential fall in the drift velocity L_v (bottom panel) as a function of Π_1 and Π_3. To extract these length scales, we used an exponential fit similar to Fig. S5. The overall trend is that with an increase in scaled cell size Π_1 and Π_3 the length scales for motility and velocity increase. The colorbar in the phase diagram is the lengthscale in μm.

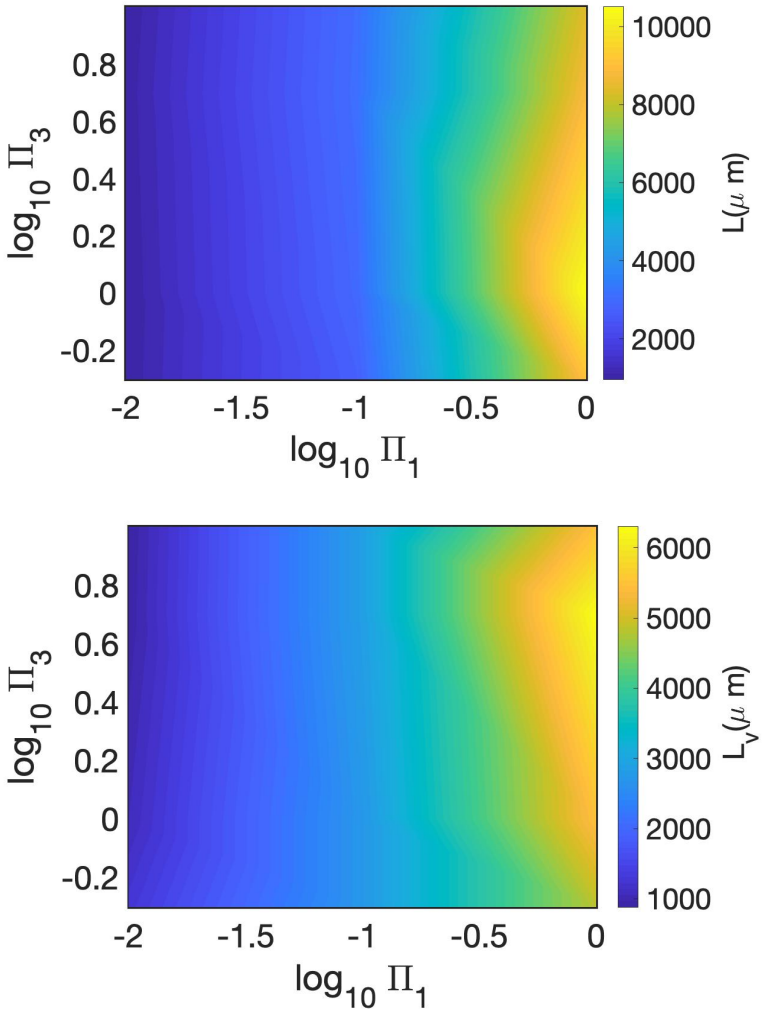

Fig. S10. Macroscopic continuum model: Phase diagrams for the decay lengthscale of motility (top panel) and decay lengthscale of drift velocity (bottom panel) as a function of Π_1 and Π_3. The colorbar shows the lengthscale in μm. These results are obtained by solving Eq. [16-20] of the main text.

References

[1] Karine Guevorkian, Marie-Josée Colbert, Mélanie Durth, Sylvie Dufour, and Françoise Brochard-Wyart. Aspiration of biological viscoelastic drops. *Physical review letters*, 104(21):218101, 2010.

[2] Isabel Palmeirim, Julien Dubrulle, Domingos Henrique, David Ish-Horowicz, and Olivier Pourquié. Uncoupling segmentation and somitogenesis in the chick presomitic mesoderm. *Dev. Gen.*, 23(1):77–85, 1998.

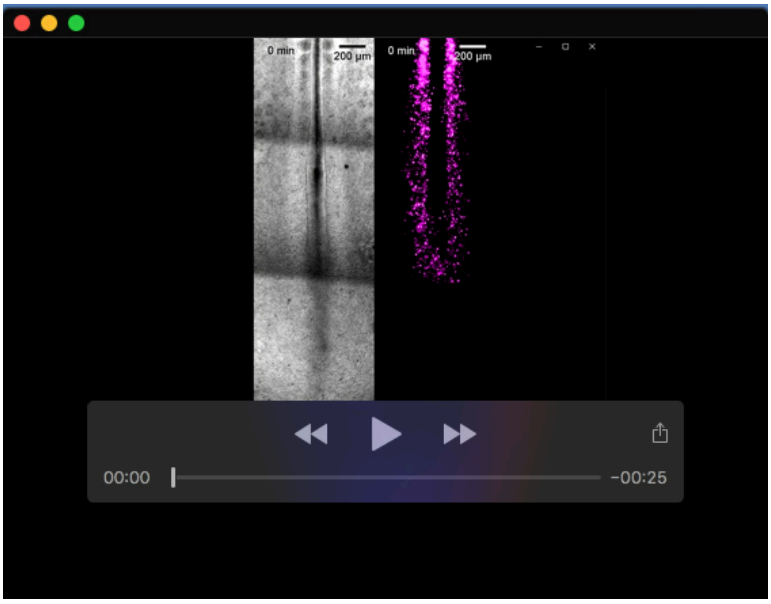

Movie 1. Video of the movement of cells by electroporating the PSM cells with fluorescent reporters specifically labeling cell nuclei in an elongating PSM.

Movie 2. Video of the cell movement in an elongating PSM from the microscpic cellular simulation. On the left we have rigid somites where cells get reflected, on the right, we have an elastic chain, representing the Tailbud, which is moving due to active pressure applied by the motile cells. The top and the bottom side has periodic boundary conditions.